Article

The Influence of CFRP Anchorage on Achieving Sectional Flexural Capacity of Strengthened Concrete Beams

Hayder A. Rasheed [1,*], Brandon R. Decker [2], Asad Esmaeily [1,†], Robert J. Peterman [1,†] and Hani G. Melhem [1,†]

[1] Department of Civil Engineering, Kansas State University, Manhattan, KS 66506, USA;
E-Mails: asad@ksu.edu (A.E.); bob@ksu.edu (R.J.P.); melhem@ksu.edu (H.G.M.)
[2] Penco Engineering, Plainville, KS 67663, USA; E-Mail: brandondecker81@gmail.com

[†] These authors contributed equally to this work.

[*] Author to whom correspondence should be addressed; E-Mail: hayder@ksu.edu;
Tel.: +1-785-532-1589; Fax: +1-785-532-7717.

Abstract: This research program is intended to verify the influence of using distributed external U-wrap CFRP anchorage to shift the failure mode from overall debonding to sectional flexural failure for concrete beams externally bonded with CFRP sheets. Premature cover delamination and FRP debonding are predominant failure modes in FRP flexural strengthening that may be delayed or prevented by using FRP anchorage. The present experimental study aims to comparatively prove that proper anchorage of flexural strengthening is anticipated to yield a classical flexural failure by FRP rupture or concrete crushing. Once the cohesion of concrete and/or the adhesion with the FRP is exhausted, the U-wraps are engaged to provide anchorage to the flexural FRP through shear friction. Accordingly, three identical T beams and three identical rectangular beams were designed and constructed to examine the capacity improvement by preventing premature debonding failure. The first specimen in each series was tested as a control beam. The second specimen in each series was strengthened using five layers of flexural CFRP in order to admit a debonding failure. The third specimen in each series was strengthened with the same five layers of flexural CFRP plus additional transverse CFRP U-wraps. This study proved that it is possible to quantify the higher flexural capacity of CFRP strengthened beams using external anchorage.

1. Introduction

Structural strengthening and repair have become a major topic of interest over the past three decades due to the infrastructural needs for rehabilitation. Externally bonded Fiber Reinforced Polymer (FRP) provides a state-of-the-art technique for strengthening and rehabilitation. Traditional methods of strengthening involve the application of externally bonded steel plates. However, the latter suffers from several shortcomings including the deterioration of bond between the steel and concrete due to steel corrosion, the difficulty in handling large steel plates, and the limited delivery lengths. Composites can provide a strengthening technique where the conventional systems do not work as efficiently. Specifically, FRP sheets can be used in place of steel plates. FRP sheets can be wrapped around a structural element to provide anchorage and ease of construction.

One drawback of the FRP flexural strengthening technique is the dominance of two premature failure modes, namely cover delamination and sheet debonding. These two modes alter the more classical sectional flexural modes of FRP rupture and concrete crushing. While developing methods to predict cover delamination, several investigators formulated empirical and analytical expressions for that purpose [1–7]. Some of these procedures yielded inconsistent results [5]. It was observed by other researchers that FRP debonding failure is still a dominant failure mode even in beams with FRP sheets extending close to the supports, where the stress concentrations are negligible or even those with end anchorage [8–12]. In this case, induced intermediate shear or flexural crack debonding is predominant. To advance the performance of FRP strengthened beams, other studies focused on various ways to prevent such premature modes of failure, among which using different external end anchorage layouts [11–14]. Recently issues raised by the use of externally bonded FRP sheets include the focus on FRP anchorage to improve the utilization of the material in strengthening of reinforced concrete members [15,16].

The present study is intended to qualify the use of a distributed CFRP anchorage system to control both cover delamination and sheet debonding for beams more prone to those failure modes by virtue of having a considerable number of layers in flexural strengthening. T beams are examined to shift their failure mode to FRP rupture and rectangular beams are tested to shift their failure mode to concrete crushing.

2. Specimen Design

2.1. Beam Geometry

The beam design was performed using a nonlinear analysis program based on the incremental deformation technique. All of the beams have a length of 4877 mm with a clear span of 4724 mm. The T beams have web dimensions of 152 mm × 305 mm with the depth extending through the flange thickness, Figure 1a. The flange dimensions are 406 mm width and 102 mm thickness. The main flexural reinforcement consists of 2 No. 5 bars. The compression steel consists of 4 No. 3 bars to hold the shear reinforcement caging Figure 1a. The ultimate moment capacity of the control T beam is calculated to be 48.78 kN-m. The rectangular beams have the same 152 mm × 305 mm cross section, Figure 1b. The

main flexural reinforcement is identical to that of the T section with two No. 3 bars used for the compression steel just to provide a caging framework for the shear reinforcement, Figure 1b. The ultimate moment capacity of the control rectangular beam is calculated to be 46.20 kN-m, which is almost identical to that of the T beam. Both the T and rectangular beams have shear reinforcement consisting of No. 3 stirrups at 127 mm on center, Figure 1a-b. The complete dimensions of the two beam sections are listed in Table 1. Despite the similar moment capacity of both the T and rectangular sections, the ultimate moment capacity of the same sections strengthened with five CFRP layers yield different failure modes and different results. This is attributed to the existence of the concrete flange that admits FRP rupture failure mode as opposed to concrete crushing in the case of the rectangular section. Nevertheless, the use of a large number of flexural CFRP layers is expected to lead to a deboning failure in the T and rectangular beams. It is the aim of this work to develop an anchorage system that shifts the debonding failure back to the FRP rupture failure in case of the T beam and concrete crushing failure in case of the rectangular beam.
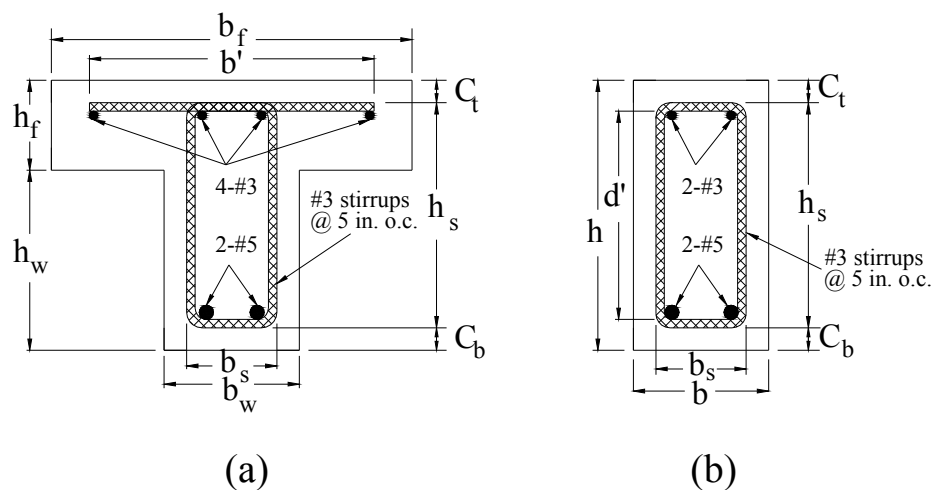
Figure 1. Beam specimen cross-section (**a**) T-beam; (**b**) rectangular beam.

Table 1. Dimensions of beam specimen cross-sections.

| Variable	Dimension
b_f	16 in (406.4 mm)
h_f	4 in (101.6 mm)
b_w	6 in (152.4 mm)
h_w	8 in (203.2 mm)
C_t	1 in (25.4 mm)
C_b	1 in (25.4 mm)
h_s	10 in (254 mm)
b'	13 in (330.2 mm)
b_s	4 in (101.6 mm)

2.2. Material Properties

The concrete that was used in casting the six beams is ready mix with a mix design nominal strength of 34.5 MPa. The average actual compressive strength of 18 test cylinders (102 mm × 203 mm) was 36.5 MPa. The material properties of the reinforcing steel were provided by the manufacturer to have a modulus of 200,000 MPa and yield strength of 483 MPa. The actual tensile testing of three samples of 203 mm long bar specimens was performed by Kansas Department of Transportation research lab. The average modulus and yield strength of the No. 3 bars were 213,180 MPa and 450.6 MPa, respectively. The average modulus and yield strength of the No. 5 bars were 204,493 MPa and 480.45 MPa, respectively.

The material properties of the V-Wrap C100 High Strength Carbon Fiber Reinforced Polymer sheets (CFRP) were provided by the manufacturer to have a modulus of 227,527 MPa, strength of 3792 MPa and sheet thickness of 0.165 mm based on the net fiber area. This corresponds to an ultimate strain of 0.017. The actual coupon tensile testing was performed based on ASTM Standard D3039. The modulus and strength averaged 59,931.6 MPa and 768.55 MPa and layer thickness of 0.7 mm based on the laminate area. These values were the average of five specimens as required by the ASTM Standard corresponding to an ultimate average strain of 0.0129.

3. Experimental Program

3.1. Test Setup and Data Acquisition

The flexural tests were performed in the structural testing laboratory of Kansas State University. The beams were loaded in four-point bending using a 1.22-m long steel spreader beam and a 222.5 kN hydraulic actuator. The actuator is controlled by a servo-hydraulic system called FlexTestGT (MTS, Eden Prairie, MN, USA). The beams were simply supported with the supports placed 75 mm from the edge of the beam, providing a clear span of 4724 mm, see Figure 2. Two-330 mm LVDT devices were placed on each side of the beam at mid-span.
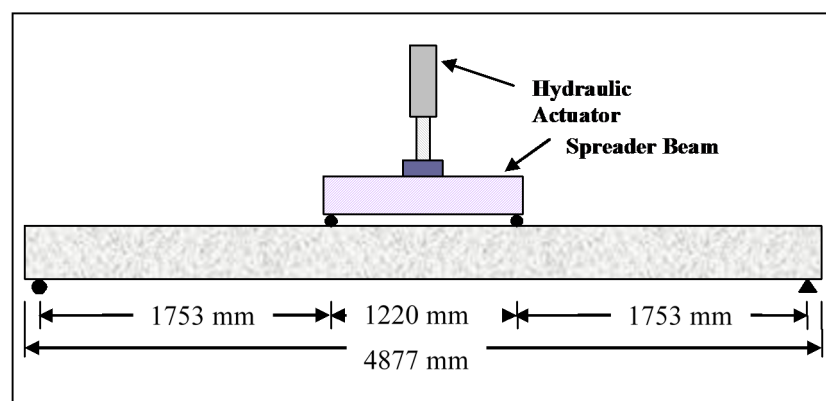
**Figure 2.** Beam profile and experimental test setup.

3.2. Test Results

3.2.1. Control T Beam (T1)

The first specimen tested in the series of T-shaped beams is the control beam (T1). The beam was loaded in load control at a rate of 2.225 kN per minute. At a load of 48.95 kN, the system was switched to displacement control at a rate of 2.54 mm per minute. From the preliminary analysis, the beam was predicted to fail at a load of approximately 54.8 kN. Flexural cracks began developing at a load of approximately 19.1 kN. The beam failed at a load of 70.75 kN. Figure 3 shows beam T1 at the end of testing. Figure 4 shows the beam load-deflection response to failure. It is evident from Figure 4 that Beam T1 has a post-yield stiffness. This was incorporated in the refined analysis resulting in a failure load of 67.42 kN. At the failure load, the deflection of the mid-span was 160 mm and the failure mode was concrete crushing in the flange at mid span, Figure 3.


Figure 3. Beam T1 at failure.
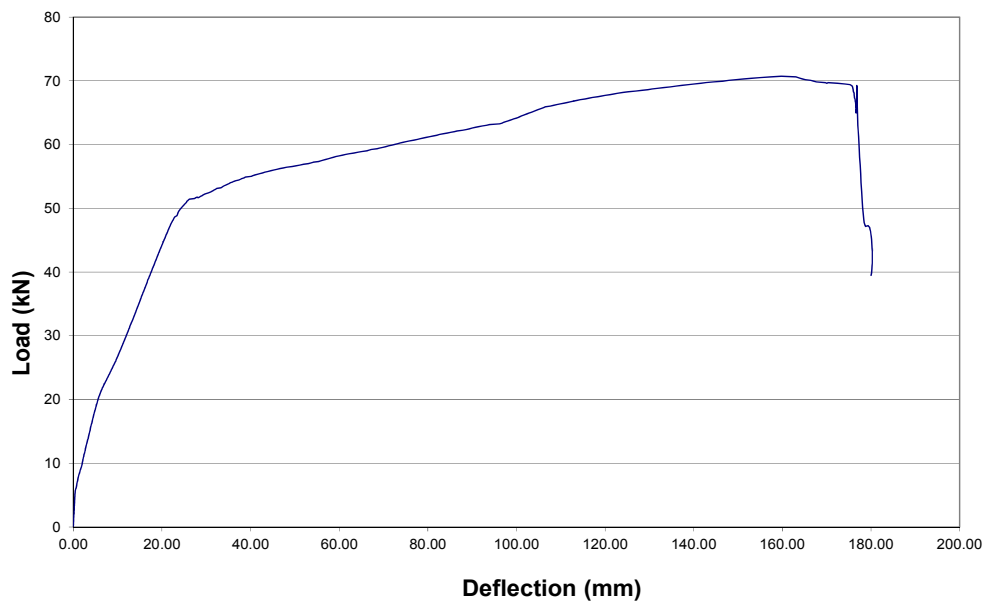
Figure 4. Load-deflection response of T1.

3.2.2. T-Beam with Flexural CFRP Only (T2)

The next beam tested is the T-beam specimen with five layers of flexural CFRP reinforcement on the bottom surface of the beam in the longitudinal direction. For the test to be considered a success, the beam had to fail at a load higher than that of the control beam. Using the Teng *et al.* [10] model of predicting FRP debonding, it was estimated that the beam would fail at a load of approximately 105.91 kN. The beam was loaded in load control at the same load rate of 2.225 kN per minute. At a load of 66.75 kN, the control system was switched to displacement control at a rate of 2.54 mm per minute. The beam reached a load of 113.74 kN when the CFRP debonded with tremendous energy release. This failure load was higher than that predicted by Teng *et al.* [10] model. At the failure load, the deflection at mid-span was approximately 51 mm which is much smaller than the 160 mm deflection of the control beam at peak load. The CFRP detached with mostly debonding failure at the interface while small areas of concrete cover delamination were seen, Figure 5. The load-deflection relationship for this beam specimen is shown in Figure 6.


Figure 5. Beam T2 at failure.
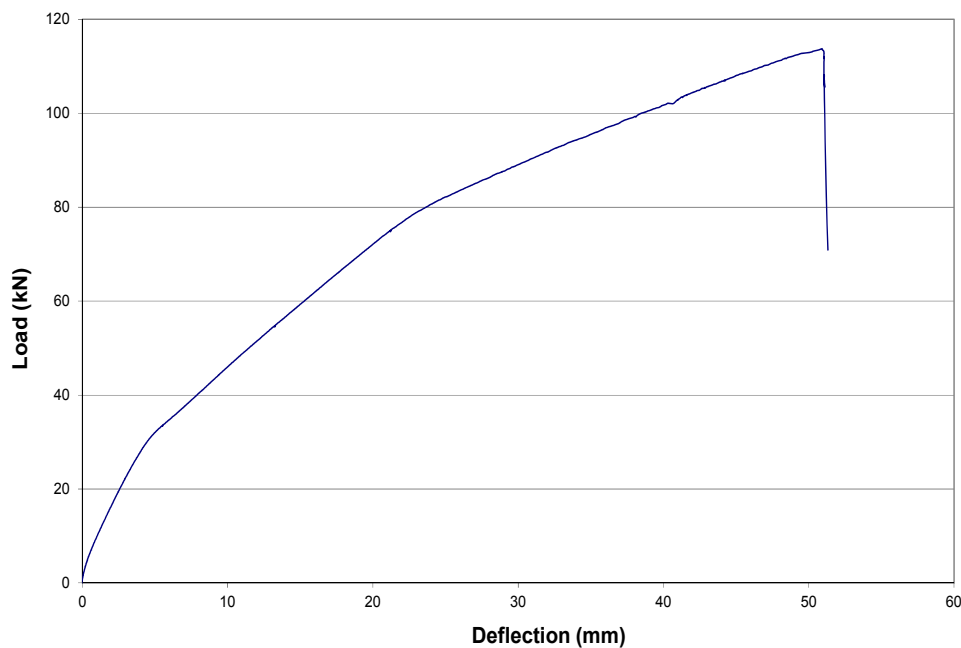
Figure 6. Load-deflection response of T2.

3.2.3. T-Beam with Flexural CFRP and U-Wrap Anchorage (T3)

The last beam tested in the series of T-beam specimens was strengthened with the same five layers of CFRP on the bottom surface of the web for flexural strength increase and it also had two layers of 127 mm wide U-shaped wraps around the web spaced at 305 mm on center. The purpose of these U-wraps was to anchor the bottom layers of CFRP in place as they tend to debond. This beam was loaded at the same rate of the previous specimens (*i.e.*, 2.225 kN per minute). The MTS system was programmed to switch to displacement control at a load of 160 kN based on the preliminary analysis results. At a load of 116 kN, about the load at which debonding occurred on beam T2, separation of the flexural CFRP sheets from the beam was evident in between the U-wraps. This was an excellent indication that the U-wraps were performing as they were supposed to by providing resistance to debonding by shear friction. The beam reached an ultimate load of 148.66 kN when the flexural CFRP sheets ruptured at mid-span, as shown in Figure 7. The failure of this beam was more drastic than the previous beams since failure occurred prior to the system switching to displacement control. Figure 8 shows the load-deflection response of beam T3.
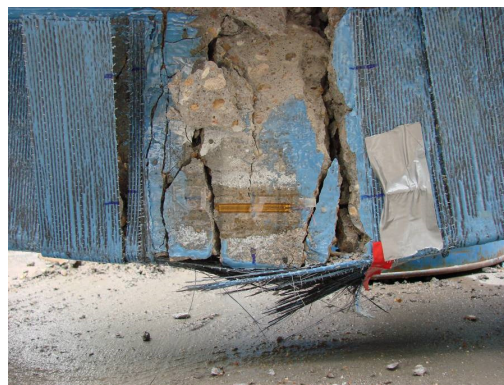

Figure 7. Beam T3 at failure.
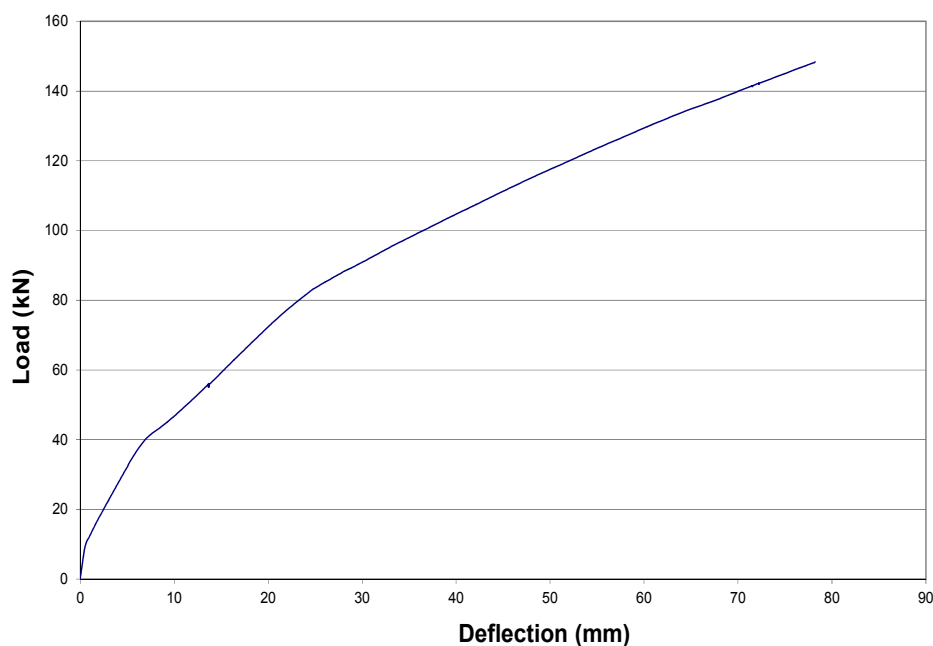
Figure 8. Load-deflection response of T3.

3.2.4. Control Rectangular Beam (R1)

The first beam tested in the series of rectangular beams is the control rectangular beam. It was determined from the flexural analysis program that the beam would fail at a load of 54 kN. The beam was loaded in load control at a rate of 2.225 kN per minute. Cracking began taking place at a load of approximately 6.68 kN. At a load of 44.5 kN, the control system was switched to displacement control to capture the correct peak load. The rate of displacement was 2.54 mm per minute. The test results show that the beam failed at a load of 54.71 kN, which is very close to the theoretical value. The beam failed in a typical mode of steel yielding followed by crushing of concrete. Figure 9 shows beam R1 after failure and Figure 10 presents the load-deflection response of the beam.
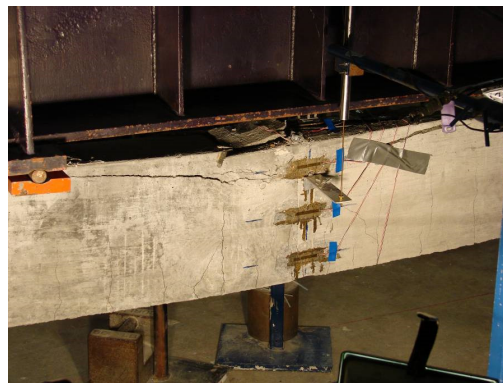
Figure 9. Beam R1 at failure.
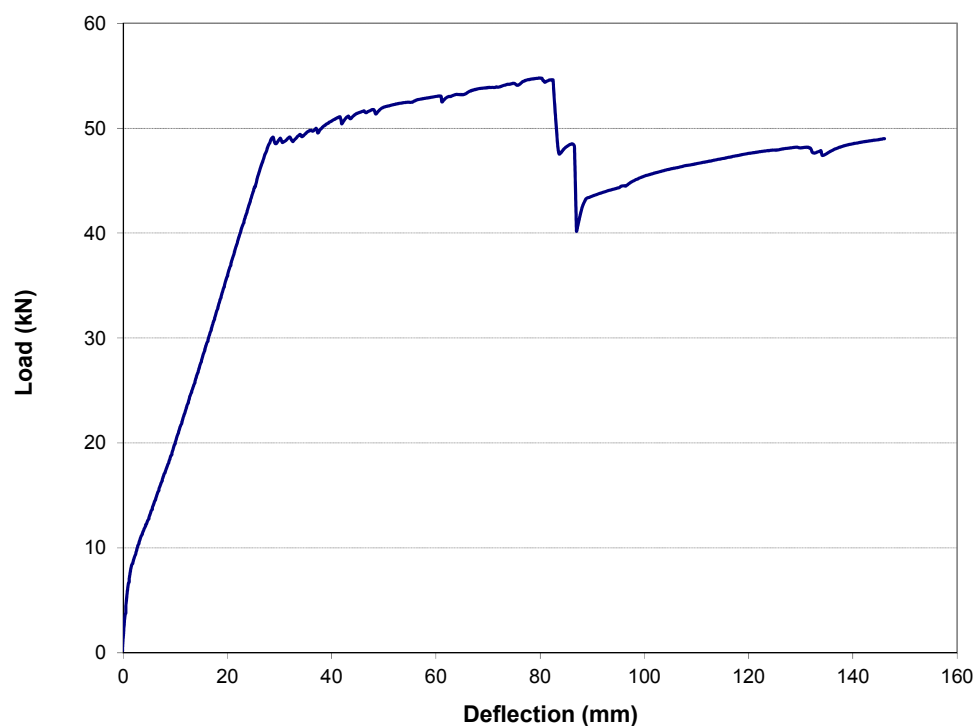
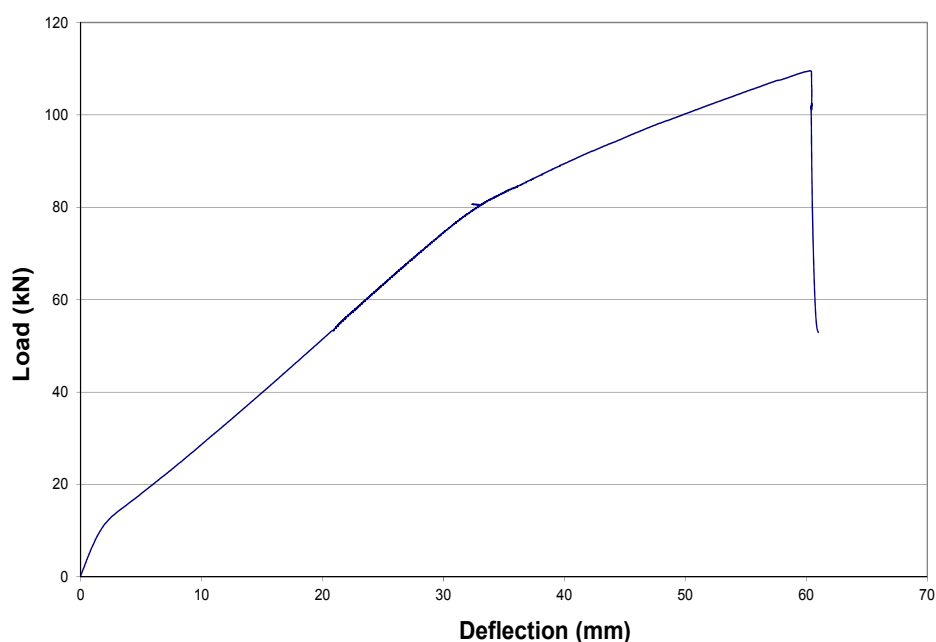**Figure 10.** Load-deflection response of R1.

3.2.5. Rectangular Beam with CFRP Only (R2)

The next step was to strengthen the second rectangular beam with five layers of flexural CFRP sheets at the bottom face. For the test to be successful, delamination had to occur at a load higher than that of the control beam, which had an ultimate load of 54.71 kN. The CFRP was predicted to debond at a load of 91.23 kN using the Teng *et al.* [10] debonding equation. The beam was loaded in load control at a rate of 2.225 kN per minute. At 53.4 kN, the system was programmed to switch to displacement control at a rate of 2.54 mm per minute. The load went well past that of the control beam. At a load of approximately 89 kN, a lot of popping sounds started coming from the FRP which indicated the occurrence of local debonding. At a load of 109.55 kN, the CFRP reinforcement debonded/delaminated with tremendous energy release. This load was higher than that predicted by Teng *et al.* [10] model, determined to be 102.84 kN, indicating a slightly conservative model in this case. The failure mode was mostly debonding failure between the CFRP and the concrete substrate as indicated by Figure 11. However, there were two small locations where the entire cover delaminated. Figure 12 shows the load-deflection results from this beam test.


Figure 11. Beam R2 at failure.

Figure 12. Load-deflection response of R2.

3.2.6. Rectangular Beam with CFRP and U-Wrap Anchorage (R3)

The last beam to test in the series of rectangular beams was the beam strengthened with the same five layers of CFRP on the soffit as beam R2 while this beam had one layer of 140 mm wide U-shaped wraps around the web spaced at 305 mm on center. The beam was loaded in load control at the same rate as the other beams. Once the test procedure was started, small cracking sounds were noticed around 26.7 kN, which seemed to be a sign of premature debonding. The noises continued throughout the test, but early debonding never occurred. At a load of 89 kN, the system was switched to displacement control. The load passed the magnitude of 109.55 kN, which is the ultimate debonding load from the previous test. This was an excellent indication that the U-wraps performed as they were supposed to by inducing resistance by shear friction once the resistance by cohesion/adhesion is lost. The failure mode was initiated by the crushing of concrete cover. The beam reached an ultimate load of 120.5 kN when the CFRP ruptured due to concrete crushing and excessive curvature at the critical section, as shown in Figure 13. This load was slightly higher than the analysis value of 116.9 kN that was predicted to be associated with the concrete extreme compression fiber reaching a strain of 0.003. Figure 14 shows the load-deflection relationship that was obtained from this test.


Figure 13. Beam R3 at failure.
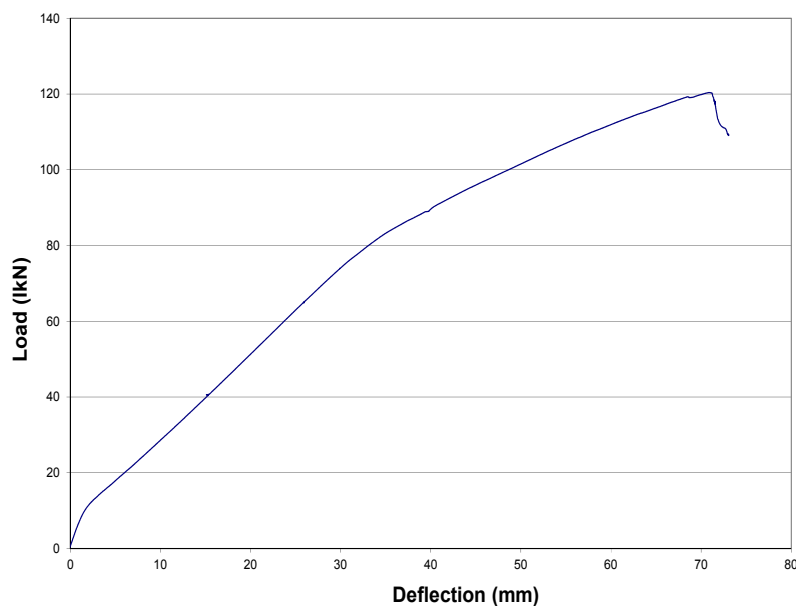
Figure 14. Load-deflection response of R3.

4. Numerical Analysis

4.1. Analysis Procedure

The incremental deformation technique for computing the moment-curvature response of the T and rectangular sections is used until the section reaches either concrete crushing at the compressive extreme fiber or the FRP rupture strain inside the CFRP sheets. Then, the integration of the moment-curvature curve along the beam is implemented, to generate the load-deflection response up to the full development of the classical sectional failure modes of concrete crushing or FRP rupture. The program is also capable of tracing the strains at different locations of the beam throughout the analysis stages. The nonlinear analysis program used in this study includes confined concrete behavior and steel post-yielding stiffness and strength. To model the confinement effects, Hognestad's parabola was only used up to ultimate unconfined strength f'_c followed by a linear descending branch to a stress level of $0.2 f'_c$ followed by a flat plateau at that residual stress, as shown in Figure 15.
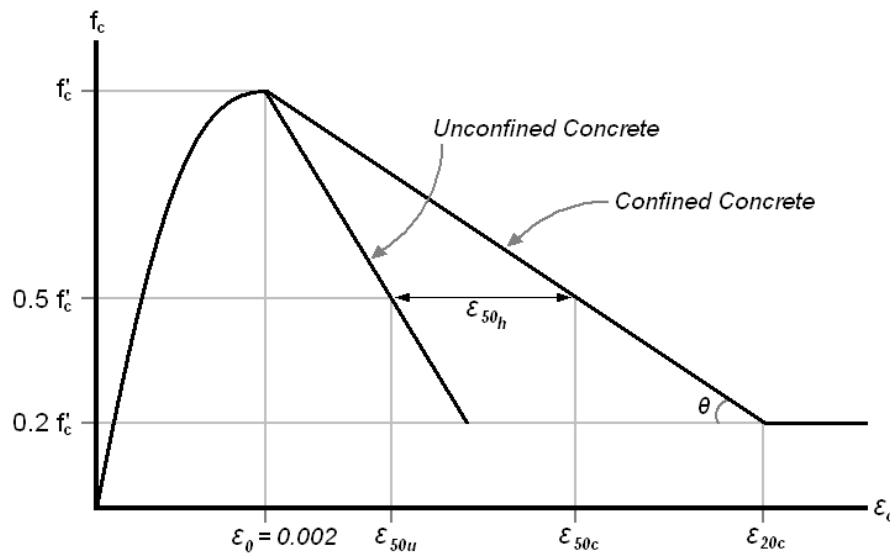
Figure 15. Confinement model for beams by Kent and Park.

The slope of the descending line was determined using the Kent and Park model, based on the level of stirrup confinement and concrete compressive strength:

$$E_{cf} = -z f'_c \tag{1}$$

$$z = \frac{0.5}{\varepsilon_{50u} + \varepsilon_{50h} - \varepsilon_0} \tag{2}$$

$$\varepsilon_{50u} = \frac{3 + \varepsilon_0 f'_c}{f'_c - 1000} \tag{3}$$

$$\varepsilon_{50h} = \frac{3}{4} \rho_s \sqrt{\frac{b''}{s_h}} \tag{4}$$

where E_{cf} is the slope of the descending branch, z is a slope multiplier, ε_{50u} is the strain of unconfined concrete corresponding to $0.5 f'_c$ and ε_{50h} is the difference between confined and unconfined concrete

strain corresponding to $0.5f'_c$, ε_0 is the strain corresponding to f'_c, ρ_s is the volumetric ratio of transverse reinforcement to concrete core measured to the outside of hoops, b'' is the width of the confined core measured to the outside of hoops, and s_h is the spacing of hoops. A bilinear stress-strain model was also used to introduce the post yield stiffness and strength, Figure 16.

$$f_s = E_s\,\varepsilon_s \qquad \text{if} \quad \varepsilon_s \leq \varepsilon_y \tag{5}$$

$$f_s = f_y + E'_s\,(\varepsilon_s - \varepsilon_y) \leq f_u \qquad \text{if} \quad \varepsilon_s > \varepsilon_y \tag{6}$$
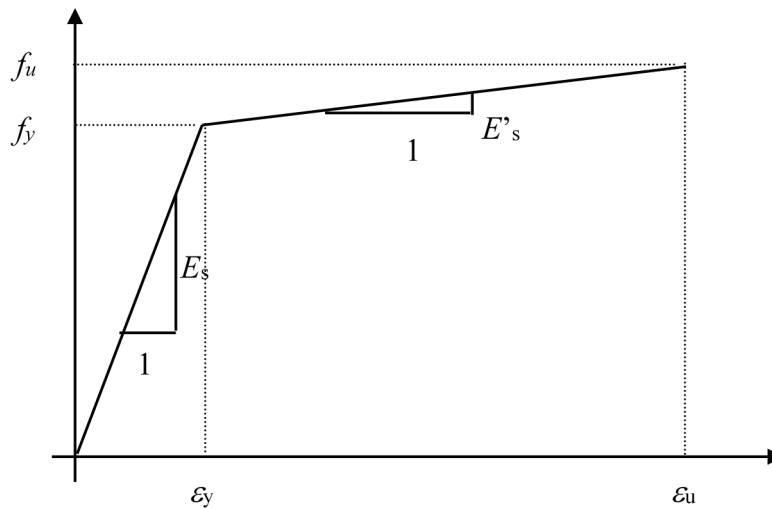
Figure 16. Stress-strain model for primary tension steel up to failure.

4.2. Nonlinear Analysis Software

Excel-based analysis software is used with a graphics user interface (GUI). In this software, the concrete section is divided into 1000 parallel fibers while having concrete in compression assume the model shown in Figure 15 and concrete in tension behave linear elastic up to brittle cracking. The reinforcing steel is provided as bars in their respective layers and is assumed to behave as shown in Figure 16. On the other hand, the FRP sheets are introduced at their respective depths allowing the wrapping of flexural FRP up and around the sides of the web, Figure 17, while the behavior of FRP is assumed to be linear-elastic up to brittle rupture. The software allows the analysis to be carried out for simple beams under three different loading conditions, namely three-point bending, four-point bending, and uniform loading as shown in Figure 18. The goal-seek functionality is used in Excel-based macros in Visual BASIC language to iterate for the roots of the nonlinear equations and solve for the neutral axis depth and moment-curvature point at every load level, Figure 19.

Reinforcement Properties					Material Properties			
Prestress	Strand Size	Number	Area	Depth		f_{ps}	300 ▾	ksi
Layer 1	No Strand ▾		0			E_{ps}	28,300	ksi
Layer 2	No Strand ▾		0			f_{pi}	182	ksi
Layer 3	No Strand ▾		0			f_{se}	165	ksi
Layer 4	No Strand ▾		0			ε_{ult}	0.05	in/in
Mild Steel	Bar Size	Number	Area	Depth				
Layer 1	#3 ▾	4	0.44	1		E_{steel}	29,000	ksi
Layer 2	#5 ▾	2	0.62	11		f_y	70	ksi
Layer 3	None ▾		0			ε_{ult}	0.04	in/in
Layer 4	None ▾		0			E2	400	ksi
Glass Bars	Area	Depth						
Layer 1						E_{glass}	7000	ksi
Layer 2						ε_{ult}	0.02	in/in
Layer 3								
Layer 4								
FRP	Width	No. Plies	Area	Depth				
Layer 1	6	5	0.195	12				
Layer 2	2	0	0			E_{FRP}	33,000	ksi
Layer 3	2	0	0			ε_{ult}	0.013	in/in
Layer 4	2	0	0		Layer Thickness		0.0065	in
Layer 5			0		Total Area		0.195	in^2
Transverse	Bar Size	Diameter	Area	Height	Width			
	#3 ▾	0.375	0.11	9.625	3.625	E_{steel}	29,000	ksi
		Spacing	Cover	h"	b"	f_y	64	ksi
		5	1	10.000	4.000	ε_{ult}	0.02	in/in
		Vhoops		Vcore	ρ"			
		2.915		200	0.014575			

Figure 17. Graphics input interface for the various reinforcements in the section.

Three Point Bending ○

L = [   ] ft
a = [   ] ft

Four Point Bending ◉

L = [15.5] ft
a = [5.75] ft

Uniform Live Load ○

L = [   ] ft

Figure 18. Graphics input interface for the various loading conditions of the beam.

Prestress	d	e	ε_1	ε_2	ε_3	ε_{Total}	f_{ps}	T	M_n
Layer 1	0.0	0.00	0.0000	-0.00252	0.00000	-0.0025	-71	0.0	0
Layer 2	0	0	0	0	0	-0.0025	-71	0.0	0
Layer 3	0	0	0	0	0	-0.0025	-71	0	0
Layer 4	0	0	0	0	0	-0.0025	-71	0	0

Mild Steel	d	ε	f_s	T	M_n
Layer 1	1	-0.00123	-35.6	-15.66	-0.31
Layer 2	11	0.01170	73.7	45.70	38.98
Layer 3	0	0	0	0	0
Layer 4	0	0	0	0	0

FRP Bars	d	ε	f_{glass}	T	M_n
Layer 1	0	0	0	0	0
Layer 2	0	0	0	0	0
Layer 3	0	0	0	0	0
Layer 4	0	0	0	0	0

FRP Wraps	d	ε_{bi}	ε	f_{FRP}	T	M_n	0.85*M_n
Layer 1	12	0.00005	0.01304	430	83.9	79	67
Layer 2	0	0.00000	0	0	0.0	0	0
Layer 3	0	0.00000	0	0	0.0	0	0
Layer 4	0	0.00000	0	0	0.0	0	0
Layer 5	0	0.00000	0	0	0.0	0	0

Reinforcement Tension	114.0	*kips*
Concrete Tension	0.4	*kips*
Concrete Compression	-114.3	*kips*
Total	**0.0**	*kips*

GoalSeek

Failure Mode — FRP Rupture   M - φ
100%   Complete   P - Δ

Mcr	9.3	*k-ft*
Mn	117.3	*k-ft*
φMn	105.5	*k-ft*

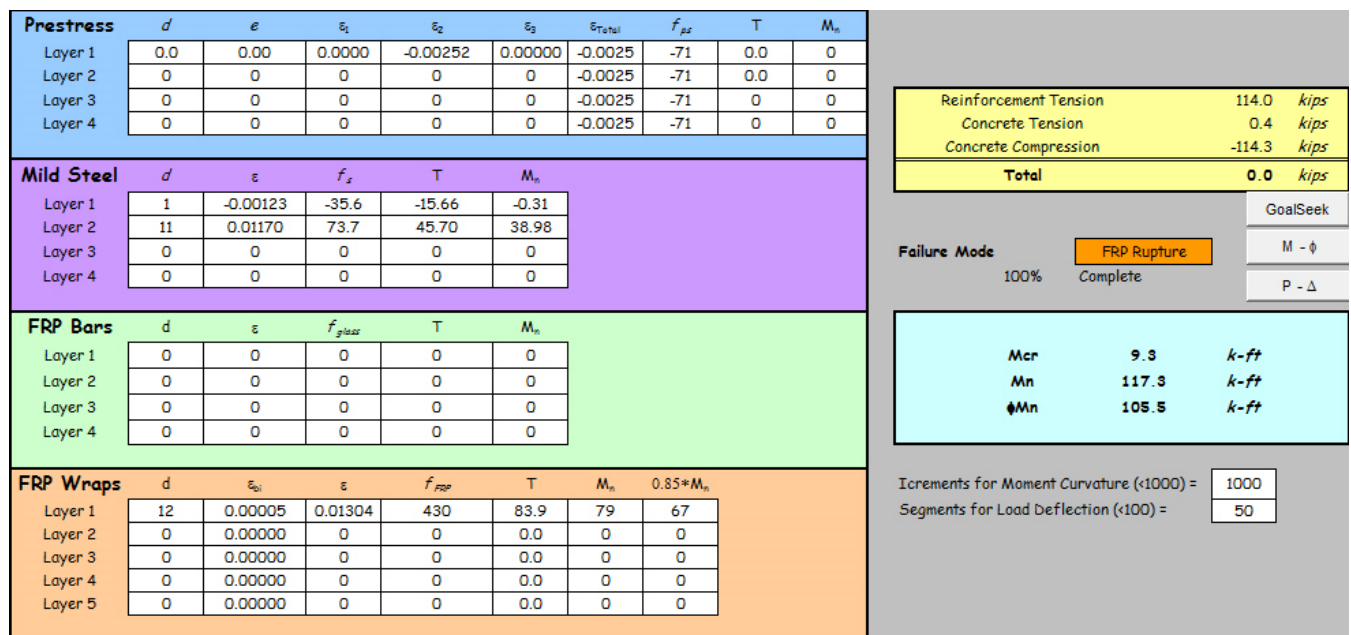| Icrements for Moment Curvature (<1000) =	1000
Segments for Load Deflection (<100) =	50

Figure 19. Run and output interface for the nonlinear beam analysis software.

4.3. Comparison with Beam Responses

The analysis procedure described above is used to compare the numerical response of the three T beams and the three rectangular beams to their corresponding experimental response curves. Figure 20 presents the comparison for the control T beam. The numerical and experimental curves are seen to match very closely up to steel yielding. After that, strain hardening was evident in both curves that showed reasonably close correspondence until failure at a load of 70.75 kN experimentally having a corresponding deflection of 160 mm. On the other hand, the analysis shows a failure load of 67.42 kN at a deflection of 244 mm indicating a shallower strain hardening response from the bilinear model. Figure 21 shows the comparison for the control rectangular beam. The numerical and experimental curves are seen to match very closely up to steel yielding as well. After that, strain hardening was also evident in both curves that showed reasonably close correspondence until failure at a load of 54.71 kN experimentally having a corresponding deflection of 79 mm. The analysis gives a failure load of 58.4 kN at a deflection of 284 mm indicating a shallower strain hardening response from the bilinear model as well. Figure 22 presents the numerical and experimental comparison for beam T2 with flexural CFRP only. The two curves are seen to be reasonably close until steel yielding. After that, they appear to be exactly matching up to the premature debonding failure that takes place at a load of 113.74 kN with a corresponding deflection of 51 mm. On the other hand, the fully developed FRP rupture failure mode is indicated numerically at a load of 173.42 kN with a corresponding deflection of 103 mm. The debonding failure load level is estimated to take place at 105.91 kN based on Teng *et al.* model [10] with a debonding strain of 0.00572. This appears to be conservative compared with the experimental finding. Figure 23 presents the numerical and experimental comparison of the response of beam R2 with flexural CFRP only. It is evident that the two curves are very closely matching up to the experimental debonding failure load which takes place at 109.55 kN corresponding to 60.3 mm deflection. On the other hand, the numerical failure load is predicted to take place at 116.93 kN corresponding to 67.7 mm deflection with concrete crushing taking place at mid-span. The debonding failure load level is estimated to take place

at 102.84 kN based on Teng *et al.* model [10] with a debonding strain of 0.00572. This appears to be slightly conservative compared with the experimental finding. Figure 24 shows the comparison of the numerical and experimental curves for beam T3 with U-wrap anchorage. It is evident that the two curves are close to each other throughout the range of loading. The experimental ultimate load in this case was increased from 113.74 kN for beam T2 to 148.66 kN in case of beam T3 with an FRP rupture failure mode at mid span. Even though the failure mode of beam T3 is FRP rupture, it failed at a load of 148.66 kN corresponding to a deflection of 79.26 mm, which is still lower than the numerical prediction of 173.42 kN with the same failure mode of FRP rupture. This is attributed to some bond slip that is expected to have taken place after the flexural CFRP debonded then was held against full separation by the U-wraps. It is very interesting to note that the moment capacity of the beam using the reduction factor (ψ_f = 0.85) implemented by the ACI 440.2R-08 [17] and applied to the contribution of the CFRP, as in Equation (5.87) of Rasheed (2014) [18], yields a failure load of 150.13 kN which is extremely close to the actual failure load of 148.66 kN. This beam test and calculation confirms the importance of using the FRP reduction factor ψ_f in determining the moment capacity for design.

Figure 25 presents the comparison of the numerical and experimental curves for beam R3 with U-wrap anchorage. It can be seen from that comparison that the two curves are in excellent agreement all the way to failure. The tested beam R3 failed at a load of 120.47 kN corresponding to a deflection of 70.4 mm. This load was indicated to take place at mid-span concrete crushing and had passed the debonding failure load of beam R2, which was 109.55 kN. On the other hand, the failure load of beam R3 was very close to that numerically predicted at concrete crushing to be 116.93 kN corresponding to a deflection of 67.7 mm, which indicates that the anchored CFRP accomplished the classical flexural capacity of the rectangular beam R3.
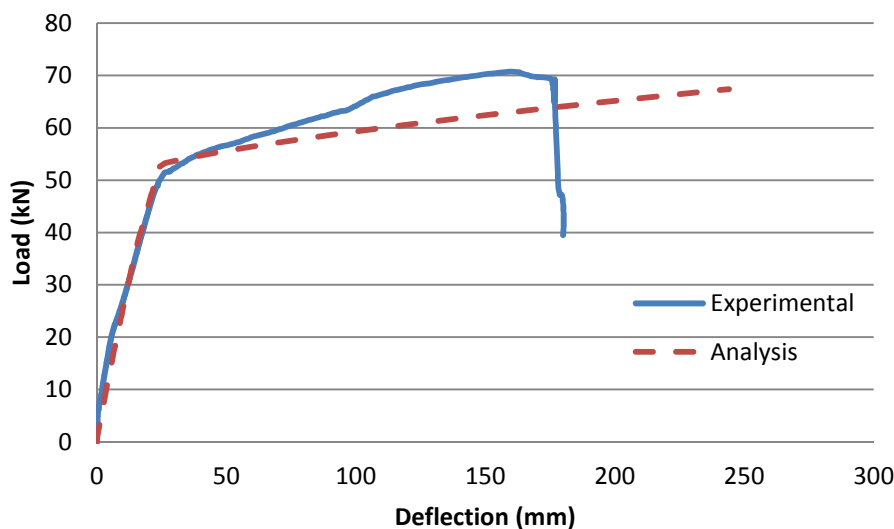
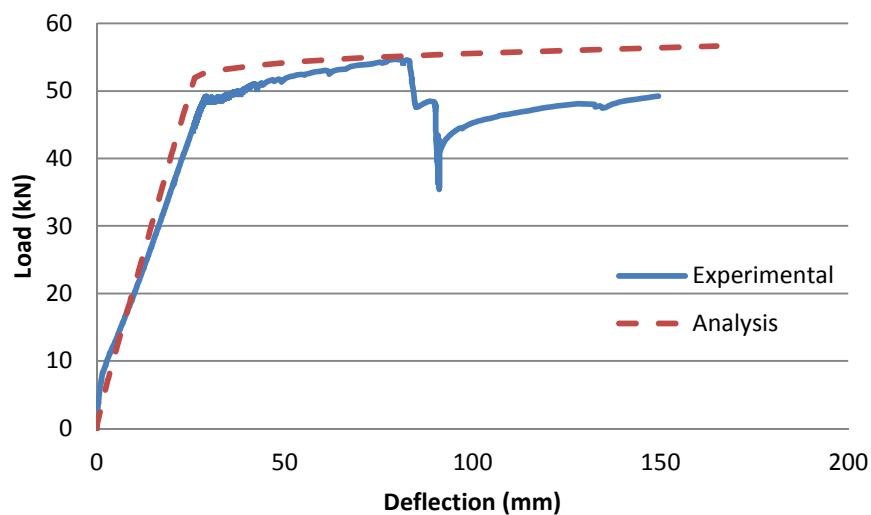**Figure 20.** Comparison of test and analysis response of T1.

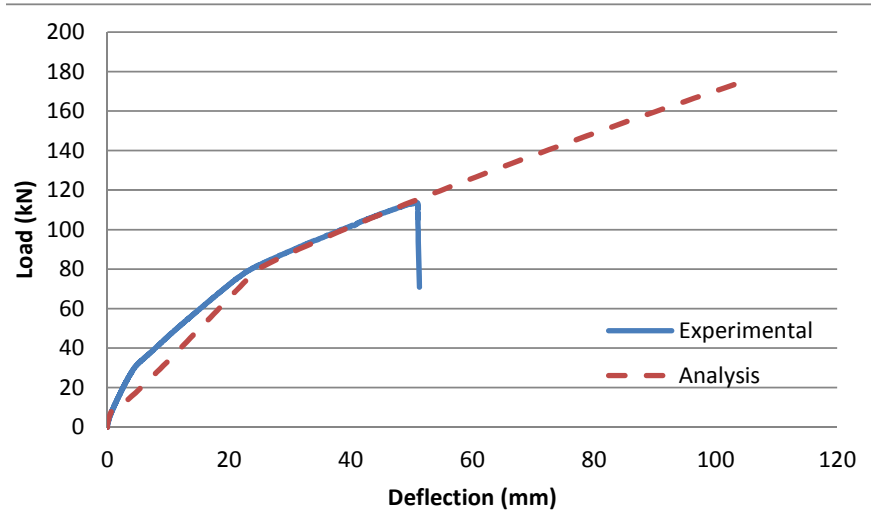**Figure 21.** Comparison of test and analysis response of R1.

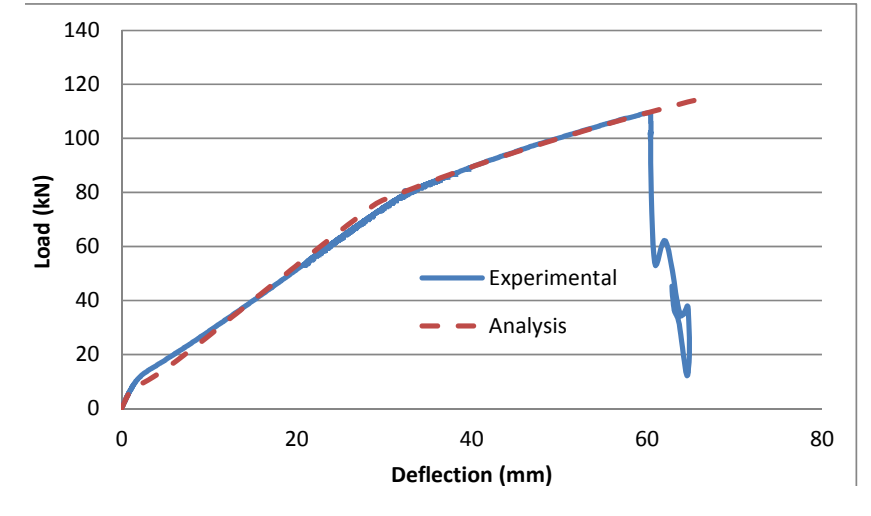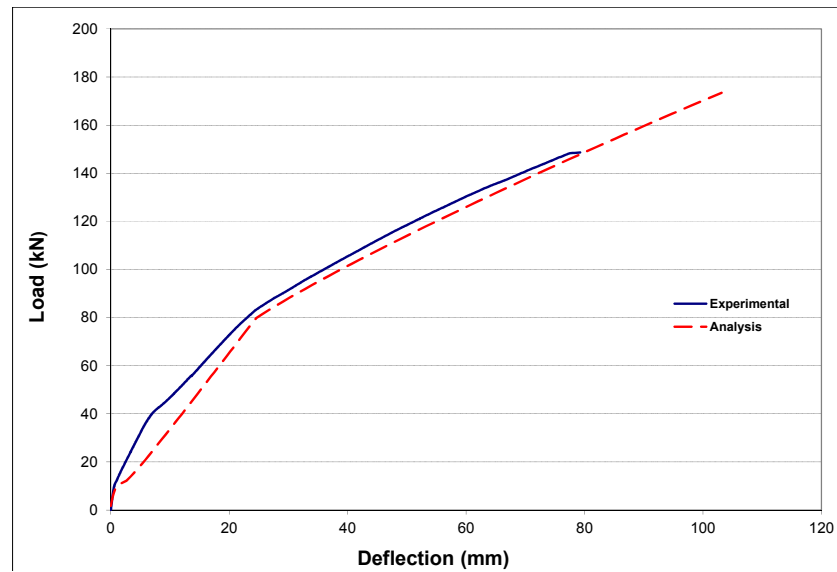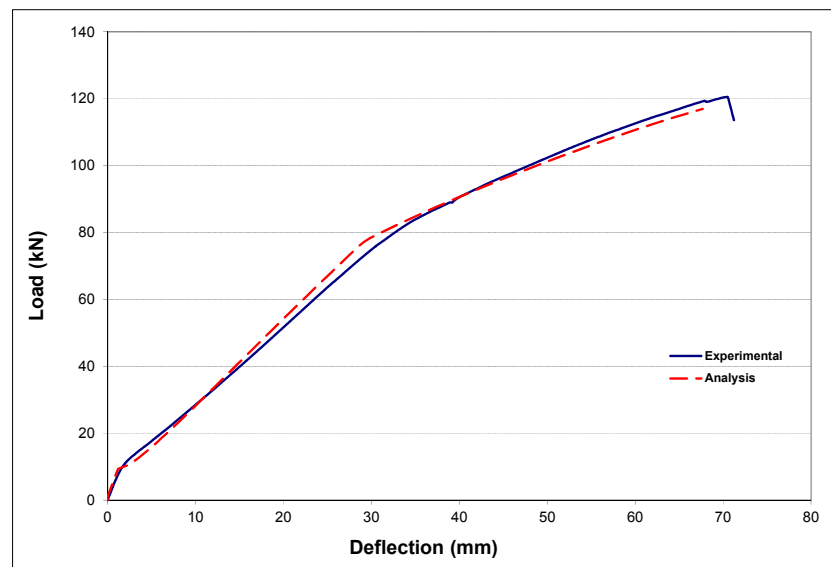**Figure 22.** Comparison of test and analysis response of T2.

Figure 23. Comparison of test and analysis response of R2.

Figure 24. Comparison of test and analysis response of T3.

Figure 25. Comparison of test and analysis response of R3.

5. Anchorage Design

5.1. Proposed Anchorage Design Procedure

To propose a design procedure that can be used to accomplish the same results obtained in this experimental study, the ACI 318-14 [19] provisions on shear friction has been adapted to yield a simplified design model. This model computes the maximum possible tensile force in the FRP at mid span corresponding to the classical sectional failure mode of FRP rupture or concrete crushing. This force needs to be developed along the FRP shear span by furnishing distributed FRP U-wrap clamps across the debonding plane, Figure 26. Accordingly, the transverse FRP area required along the shear span is that producing enough tension to control the shear friction. The proposed design procedure is summarized in the following steps:

1. Compute the maximum possible FRP tensile force that needs to be developed at the level of classical sectional failure moment:

$$T_f = E_f A_f \varepsilon_{fu} \text{ (FRP Rupture)} \tag{7}$$

$$T_f = E_f A_f \left[0.003 \left(\frac{d_f}{c} - 1 \right) - \varepsilon_{bi} \right] \text{ (Concrete Crushing)} \tag{8}$$

2. Compute the horizontal shear force per unit length of shear span:

$$V_{sf} = \frac{T_f}{L_{af}} \tag{9}$$

where V_{sf} is the horizontal shear friction force per unit length of the FRP shear span, and L_{af} is the FRP shear span.

3. Compute the clamping tension force per unit length in the transverse FRP direction using the shear friction expression:

$$V_{sf} = \mu T_{sf} \xrightarrow{\text{yields}} T_{sf} = \frac{V_{sf}}{\mu} \tag{10}$$

4. Compute the clamping tension force per unit length in the transverse FRP direction. ACI 440.2R-08 [17] limits the effective FRP transverse strain ε_{fe} to less than 0.004. In this model, $\varepsilon_{fe} = 0.003$ is assumed:

$$T_{sf} = \phi A_{vf} E_f \varepsilon_{fe} \xrightarrow{\text{yields}} A_{vf} = \frac{T_{sf}}{0.85 E_f (0.003)} = 392.2 \frac{T_{sf}}{E_f} \tag{11}$$

5. Compute the width and the number of layers for the transverse FRP:

$$A_{vf} = 2 n t_f w_f \xrightarrow{\text{yields}} w_f = 196.1 \frac{T_{sf}}{n E_f t_f} \tag{12}$$
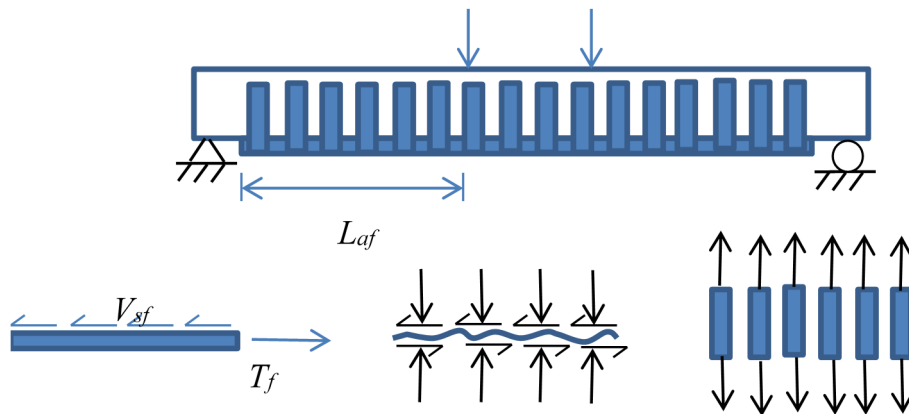
Figure 26. Schematic showing the shear friction mechanism in stretching the transverse FRP.

5.2. Anchorage Design Details

The following are the design calculations for the anchors used with T3 and R3 beams:

5.2.1. Beam T3: FRP Rupture Failure Mode

$$T_f = 227.527 \times 5 \times 152.4 \times 0.165 \times 0.0129 = 369.03 \text{ kN}$$

$$V_{sf} = \frac{369.03}{1.676} = 220.2 \text{ kN/m}$$

$$T_{sf} = \frac{220.2}{1.4} = 157.3 \text{ kN/m}$$

$$w_f = 196.1 \frac{157.3 \text{ kN/m}}{2 \times 227.527 \times 0.165} = 410.8 \text{ mm/m}$$

Use 2 layers of 127 mm wide U-wraps at a spacing of 305 mm on center (416 mm/m).

5.2.2. Beam R3: Concrete Crushing Failure Mode

From force equilibrium, c = 102 mm.

$$T_f = 227.527 \times 5 \times 152.4 \times 0.165 \times \left[0.003 \times \left(\frac{305}{102} - 1 \right) - 0 \right] = 170.8 \text{ kN}$$

$$V_{sf} = \frac{170.8}{1.676} = 101.9 \text{ kN/m}$$

$$T_{sf} = \frac{101.9}{1.4} = 72.8 \text{ kN/m}$$

$$w_f = 196.1 \frac{72.8 \text{ kN/m}}{1 \times 227.527 \times 0.165} = 380 \text{ mm/m}$$

Use 1 layer of 140 mm wide U-wraps at a spacing of 305 mm on center (459 mm/m).

6. Conclusions

An experimental program is conducted to qualify the performance of a distributed CFRP anchorage system in controlling the deboning failure mode in T and rectangular beams leading to the attainment of the full flexural capacity. The results indicate the success of the technique in achieving its goals and the applicability of the Teng *et al.* [10] model, implemented by the ACI 440.2R-08 [17], in conservatively predicting the debonding failure. The analysis program implemented is also shown to yield excellent correspondence to the overall experimental response. A shear friction model adapted from ACI 318-14 [19] is proposed to compute the CFRP transverse U-wraps needed to effectively anchor the large number of flexural layers used. This model has yielded two different U-wrap designs that worked in achieving the classical sectional failure for both the T and rectangular beams. This study further confirmed the importance of using the FRP reduction factor ψ_f in determining the ultimate moment capacity for design.

Author Contributions

Hayder A. Rasheed designed the experiments and performed the analyses. Brandon R. Decker built the specimens and conducted the experiments. Asad Esmaeily, Robert J. Peterman and Hani G. Melhem helped in performing the experiments and collecting the data.

Conflicts of Interest

The authors declare no conflict of interest.

References

1. Roberts, T. Approximate analysis of shear and normal stress concentrations in the adhesive layer of plated RC beams. *Struct. Eng.* **1989**, *67*, 228–233.
2. Quantrill, R.; Hollaway, L.; Thorne, A. Predictions of the maximum plate end stresses of FRP strengthened beams: Part II. *Mag. Concr. Res.* **1996**, *48*, 343–351.
3. Täljsten, B. Strengthening of beams by plate bonding. *J. Mater. Civ. Eng.* **1997**, *9*, 206–212.
4. Malek, A.; Saadatmanesh, H.; Ehsani, M. Prediction of failure load of R/C beams strengthened with FRP plate due to stress concentration at the plate end. *ACI Struct. J.* **1998**, *95*, 142–152.
5. El-Mihilmy, M.; Tedesco, J. Prediction of anchorage failure for reinforced concrete beams strengthened with fiber-reinforced polymer plates. *ACI Struct. J.* **2001**, *98*, 301–314.
6. Rasheed, H.A.; Perviaz, S. Bond slip analysis of FRP strengthened beams. *J. Eng. Mech.* **2002**, *128*, 78–86.
7. Rasheed, H.A.; Larson, K.H.; Nayyeri Amiri, S. Analytical Solution of Interface Shear Stresses in Externally Bonded FRP-Strengthened Concrete Beams. *J. Eng. Mech.* **2013**, *139*, 18–28.
8. Ross, C.; Jerome, D.; Tedesco, J.; Hughes, M. Strengthening of reinforced concrete beams with externally bonded composite laminates. *ACI Struct. J.* **1999**, *96*, 212–220.
9. Fanning, P.; Kelly, O. Ultimate response of RC beams strengthened with CFRP plates. *J. Compos. Construct.* **2001**, *5*, 122–127.
10. Teng, J.G.; Smith, S.T.; Yao, J.; Chen, J.F. Intermediate crack-induced debonding in RC beams and slabs. *Construct. Build. Mater.* **2003**, *17*, 447–462.
11. Chahrour, A.; Soudki, K. Flexural response of reinforced concrete beams strengthened with end-anchored partially bonded carbon fiber-reinforced polymer strips. *J. Compos. Construct.* **2005**, *9*, 170–177.
12. Ceroni, F.; Pecce, M.; Matthys, S.; Taerwe, L. Debonding strength and anchorage devices for reinforced concrete elements strengthened with FRP sheets. *Compos. B Eng.* **2008**, *39*, 429–441.
13. Rasheed, H.A.; Nassajy, M.; Al-Subaie, S.; Abrishamchian, S.M.; Al-Tamimi, A. Suppressing Delamination Failure Mode in Concrete Beams Strengthened with Short CFRP Laminates. *Mech. Adv. Mater. Struct.* **2011**, *18*, 194–200.

14. Al-Tamimi, A.K.; Hawileh, R.; Abdalla, J.; Rasheed, H.A. Effects of Ratio of CFRP Plate Length to Shear Span and End Anchorage on Flexural Behavior of SCC R/C Beams. *ASCE J. Compos. Construct.* **2011**, *15*, 908–919.

15. Grelle, S.V.; Sneed, L.H. Review of Anchorage Systems for Externally-Bonded FRP Laminates. *Int. J. Concr. Struct. Mater.* **2013**, *7*, 17–33.

16. Kalfat, R.; Al-Mahaidi, R.; Smith, S.T. Anchorage devices used to improve the performance of reinforced concrete beams retrofitted with FRP composites: State-of-the-art review. *ASCE J. Compos. Construct.* **2013**, *17*, 14–33.

17. *Guide for the Design and Construction of Externally Bonded FRP Systems for Strengthening Concrete Structures*; ACI Committee 440.2R-08; American Concrete Institute: Farmington Hills, MI, USA, 2008.

18. Rasheed, H.A. *Strengthening Design of Reinforced Concrete with FRP*; CRC Press: Boca Raton, FL, USA, 2014.

19. *Building Code Requirements for Structural Concrete and Commentary*; ACI Committee 318; American Concrete Institute: Farmington Hills, MI, USA, 2014.